Desalination and Water Treatment
www.deswater.com

doi: 10.5004/dwt.2018.21981

108 (2018) 268–278
March

Enhancement of Cr(VI) removal from aqueous solution by carboxymethyl chitosan coated nano-zero-valent iron beads

Yanhua Xie*, Lulu Zhang, Lulu Ren, Jinglong Yang, Xueqian Zhu, Yan Yi, Tingheng Zhou

State Key Laboratory of Geohazard Prevention and Geoenvironment Protection, Chengdu University of Technology, Chengdu 610059, China, emails: xieyanhua10@cdut.cn (Y. Xie), 1240523000@qq.com (L. Zhang), 1538751481@qq.com (L. Ren), 823319874@qq.com (J. Yang), 707378930@qq.com (X. Zhu), 865204105@qq.com (Y. Yi), 1223517162@qq.com (T. Zhou)

Received 18 August 2017; Accepted 30 January 2018

ABSTRACT

Stabilized nano-zero-valent iron (nZVI) was obtained by using carboxymethyl chitosan (CMCS) as a coating agent. The performance of the composite beads was tested by Cr(VI) removal from aqueous solution. The samples were characterized by transmission electron microscopy, scanning electron microscopy, and vibrating sample magnetometry to understand their properties. The influence of various experimental conditions such as CMCS-nZVI dosage, initial Cr(VI) concentration, solution pH, and reaction temperature on Cr(VI) removal was investigated. Fourier-transform infrared spectroscopy, X-ray diffractometry, and X-ray photoelectron spectroscopy were used to explain possible reaction mechanisms. Transmission electron microscopy showed that the average diameter of iron nanoparticle was 25.35 ± 7.11 nm, and that the nanoparticles were distributed evenly on the CMCS bead surface. The saturation magnetization of the composite was 23.5 emu/g and thus the beads could be separated easily by a magnet. An increased CMCS-nZVI dosage could improve the removal efficiency of Cr(VI) and shorten the reaction time. A lower solution pH and higher temperature favored Cr(VI) removal. The Cr(VI) removal kinetics followed the pseudo-first-order model well. Cr(VI) removal by CMCS-nZVI beads may be a complex process, which includes adsorption, reduction, and chelation.

Keywords: Carboxymethyl chitosan; Nano-zero-valent iron; Hexavalent chromium; Reduction

1. Introduction

Hexavalent chromium compounds are extensively used in the manufacturing industry, especially in the leather, textile, printing and dyeing, and automobile-manufacturing industries [1]. Chromium contamination discharged by these industries has resulted in the pollution of surface water, soil, and groundwater [2]. Cr(VI) may have short- and long-term adverse effects on humans, animals, and plants [3,4]. The disposal cost of Cr(VI) as a carcinogenic teratogenic factor is relatively high [5,6]. Various treatment technologies have been developed for Cr(VI) remediation in water, including adsorption, ion exchange, flocculation precipitation, oxidation reduction, and microorganism and phytoremediation [7–10]. Considering that the toxicity and solubility of Cr(VI) is greater than that of Cr(III), more effective technologies that can rapidly and thoroughly reduce Cr(VI) to Cr(III) are required.

The high reactivity and strong reducibility of nano-zero-valent iron (nZVI) have indicated that it is effective for the removal/degradation of a wide range of pollutants, including halohydrocarbon, azo dyes, aromatic compounds, perchlorate, and heavy metals of Cu(II), Ni(II), Pb(II), and Cr(VI) [11–13]. nZVI has a small particle size and a large specific surface area, which contributes to increasing reaction rates. However, the following shortcomings exist in the

* Corresponding author.

practical application of nZVI particles: (1) because of magnetic interactions and van der Waals attractive forces, bare nZVI may form large particles by agglomeration within a few minutes, resulting in a decrease in its specific surface area and eventually a decrease in its dispersibility and reaction efficiencies [14]; and (2) the nZVI particles have a poor stability and are easily oxidized or even experience spontaneous combustion in air [15,16]. Due to the occurrence of these defects in the use of nZVI particles, it is necessary to modify their surface for convenient practical applications.

To prevent nZVI-particle aggregation and oxidization, many materials, including "green" biopolymers [17,18], resins [19,20], and clay [21] have been used as a stabilizer or supporter. Chitosan as an important natural polymer has a large number of $–NH_2$ and –OH groups in its molecular chain, which can chelate with a variety of metal ions [22,23]. It has been used as a stabilizer to enhance the dispersibility and stability of nZVI [24,25]. Liu et al. [2] used the chitosan coated nZVI beads to remove hexavalent chromium from wastewater. Entrapment of nZVI in chitosan beads could effectively prevent the particles from aggregation and oxidation. Cr(VI) adsorbed on the surface or inside of the CS-nZVI beads was quickly reduced to Cr(III), and the Cr(VI) removal efficiency reached 70.4%.

However, chitosan is insoluble in water which limits its practical application. Carboxymethyl chitosan (CMCS) as a derivative of chitosan has a better biocompatibility [26,27]. Carboxymethylation destroys the chitosan crystal structure and increases its amorphous nature [28]. The introduction of carboxyl groups in the molecular chain of chitosan allows CMCS to exhibit a better adsorption/chelation capacity for heavy metal ions (Cu, Cd, Cr, etc.) [29,30].

In this study, CMCS was chosen as a support for nZVI particles because of its dispersibility characteristics and good affinity for heavy metals. The stabilization nZVI in CMCS (CMCS-nZVI) was tested to remove Cr(VI) from water. The rate and extent of Cr(VI) degradation by CMCS-nZVI were investigated. The influence of CMCS-nZVI dosage, initial Cr(VI) concentration, solution pH, and reaction temperature on Cr(VI) removal was studied in detail. Finally, the possible mechanism of Cr(VI) degradation by CMCS-nZVI was discussed.

2. Materials and methods

2.1. Chemicals

The reagents used in this study, including $FeSO_4·7H_2O$, $NaBH_4$, $K_2Cr_2O_7$, $CaCl_2$, HCl, NaOH, and NaCl, were of analytical grade and were purchased from Sinopharm Chemical Reagent Co., Ltd. (Shanghai, China). *N*-Carboxymethyl chitosan was provided by Qiming Biological Technology Co., Ltd. (Shanghai, China), with a deacetylation degree above 80%. Deionized water was used to prepare all solutions.

2.2. CMCS-nZVI preparation

CMCS-nZVI was prepared by reducing ferrous ions with borohydride in an aqueous phase. The synthetic method was modified based on previous researches [2,31]. The preparation reaction was carried out in a 500 mL three-necked flask with mechanical stirring at 500 rpm under nitrogen gas. The flask was immersed in a water bath at 22°C ± 1°C. Ferrous sulfate ($FeSO_4·7H_2O$, 4.98 g) was dissolved with 45 mL deaerated water and 45 mL anhydrous ethanol. The solution was stirred for 15 min to achieve complete dissolution. Sodium borohydride ($NaBH_4$, 0.8 mol/L) solution was dropped into the mixture at a flow rate of 0.15 mL/s. The suspension was stirred for 15 min until hydrogen-gas generation ceased. The resultant nZVI particles were separated magnetically and washed several times with deoxygenated water to remove residual chemicals. Fresh nZVI particles were added to 50 mL 5% CMCS solution, and dispersed ultrasonically for 10 min. Suspension (1 mL) was dropped into 20 mL 9% $CaCl_2$ solution that contained 50% (v/v) ethanol by an injector, and the CMCS-nZVI beads were formed. After cross-linking for 1 h, the CMCS-nZVI beads were washed with deaerated water, dried under vacuum at 70°C ± 1°C, and stored under anaerobic conditions.

2.3. Hexavalent chromium-removal experiments

Hexavalent chromium-removal experiments were conducted in a series of duplicated batch experiments. Batch tests were carried out in 100 mL serum bottles capped with a Teflon/silicone mininert valve. To each bottle, 50 mL Cr(VI) solution at the desired concentration and CMCS-nZVI dosage were added under nitrogen gas. The bottle was sealed with the Teflon/silicone mininert valve. Sealed bottles were placed in a water bath shaker at 200 rpm. Samples were collected at a given reaction interval and filtered through a 0.22 μm filter for Cr(VI) analysis. The main influencing factors, including temperature (25°C ± 1°C, 40°C ± 1°C, and 50°C ± 1°C), CMCS-nZVI bead dosage (0.12–0.6 g/L), initial Cr(VI) concentration (5–50 mg/L), and solution pH (3–11), were studied in detail. Control experiments were carried out without CMCS-nZVI addition under other identical conditions.

2.4. CMCS-nZVI characterization and analytical methods

The surface morphologies of the CMCS-nZVI beads were studied using field-emission transmission electron microscopy (TEM; Tecnai G2F20, Hillsboro, OR, USA) and scanning electron microscopy (SEM; Quanta 250 FEG, Hong Kong, China). An vibrating sample magnetometry (VSM; MPMS-XL-7, San Diego, California, USA) was used to characterize the magnetic properties of the CMCS-nZVI beads at room temperature. Fourier-transform infrared (FTIR) spectra of the CMCS-nZVI beads (before and after reaction) were obtained with an FTIR spectrometer (Magna-IR750, Nicolet, Madison, WI, USA). The CMCS-nZVI samples (before and after reaction) were analyzed by X-ray diffractometry (XRD; D8 Advance, Karlsruhe, Germany) and X-ray photoelectron spectroscopy (XPS; Thermo ESCALAB 250XI, Maple Plain, MN, USA) to study the surface state and transformation of the composite beads. The Cr(VI) concentration in solution was determined by the diphenylcarbazine method using an ultraviolet/visible spectrophotometer.

3. Results and discussion

3.1. TEM analysis

The macroscopic shape of the CMCS-nZVI beads is shown in Fig. 1(a). The CMCS-nZVI beads appeared black, which is attributed to nZVI particle entrapment in the CMCS

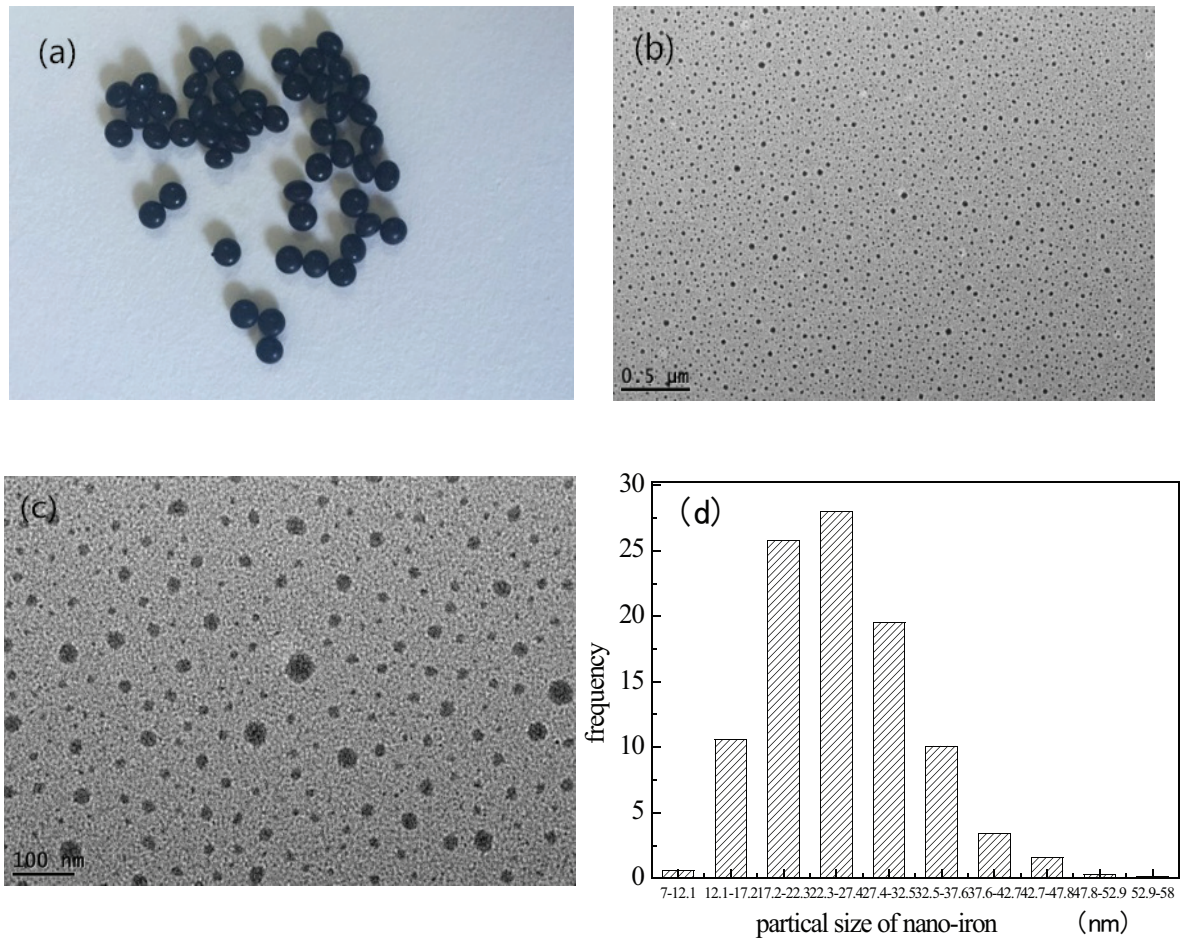

Fig. 1. The macroscopic shape of CMCS-nZVI beads (a), TEM images of CMCS-nZVI beads in proportion of 0.5 μm (b) and 100 nm (c), and size distribution of nZVI particle (d).

gel beads. The black beads were almost spherical with a mean diameter of 3 mm. Figs. 1(b) and (c) show TEM images of the CMCS-nZVI beads with different magnification times. The TEM images show that the black nanoiron particles are distributed uniformly on the gel bead surface, and agglomeration does not occur during synthesis. This result confirmed that the *N*-carboxymethyl chitosan could increase the nZVI dispersibility to a certain degree. Fig. 1(c) shows some nZVI particles with a relatively larger particle size covered by a thin gray layer. This is considered to be the core–shell structure where the core is attributed to Fe^0, whereas the shell probably results from iron oxides. In general, the thickness of freshly prepared nZVI layers ranges from 2 to 5 nm [32]. Approximately, 2136 of the fresh nZVI particles were selected at random to determine the nZVI particle-size distribution and the results are shown in Fig. 1(d). The size of the nZVI particles on the gel beads ranged from 7 to 58 nm, with an average particle size of 25.35 ± 7.11 nm.

3.2. SEM analysis

Figs. 2(a) and (b) show SEM images of fresh CMCS-nZVI beads with different magnification times. Fig. 2(a) shows that the fresh CMCS-nZVI beads are regular spheres with a compact surface, which agrees with the research results of Gujarathi et al. [33]. Fig. 2(b) shows that many spherical iron nanoparticles are distributed on the gel-bead surface. Some hexahedra particles exist on the bead surface, and are attributed to iron oxides [34], which agree with the TEM results. The reason may be the fact that a few iron nanoparticles on the bead surface were oxidized by oxygen in water or air during the transportation, conservation, and detection process. However, few iron-oxide particles were present, which indicated that *N*-carboxymethyl chitosan could protect iron nanoparticles from oxidation. Figs. 2(c) and (d) show SEM images of CMCS-nZVI beads after reaction with Cr(VI). Compared with the compact surface of newly prepared CMCS-nZVI beads, the gel-bead surface became rough and irregular after reaction with Cr(VI). The iron nanoparticles on the gel beads disappeared and changed to a grape-like chain, which indicates that a series of chemical reactions occurred and iron nanoparticles were oxidized to iron oxides.

3.3. VSM analysis

VSM was used to study the magnetic properties of the CMCS-nZVI beads. Fig. 3(a) shows the hysteresis loops of naked nZVI and CMCS-nZVI beads. Fig. 3(b) shows the magnetic recovery of the CMCS-nZVI beads. The coercivity and remanence of naked nZVI particles and CMCS-nZVI beads

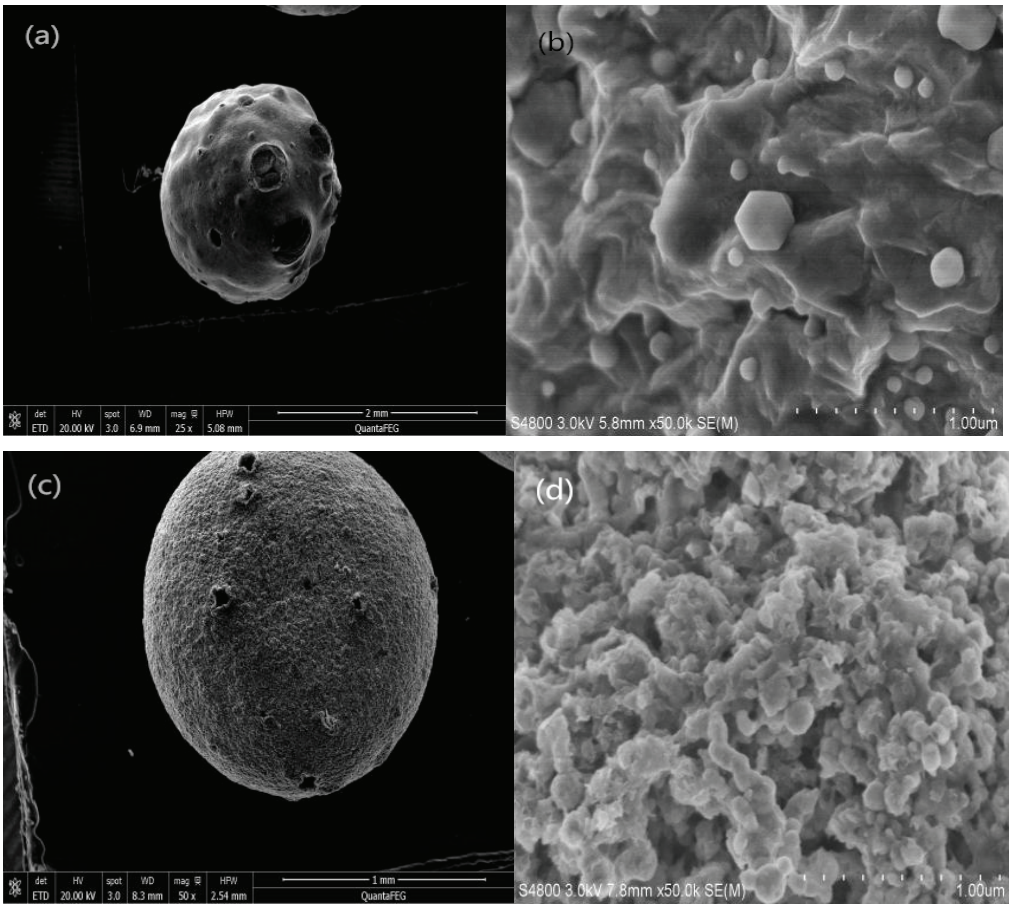

Fig. 2. SEM images of CMCS-nZVI beads before (a) and (b) and after (c) and (d) reaction with Cr(VI).

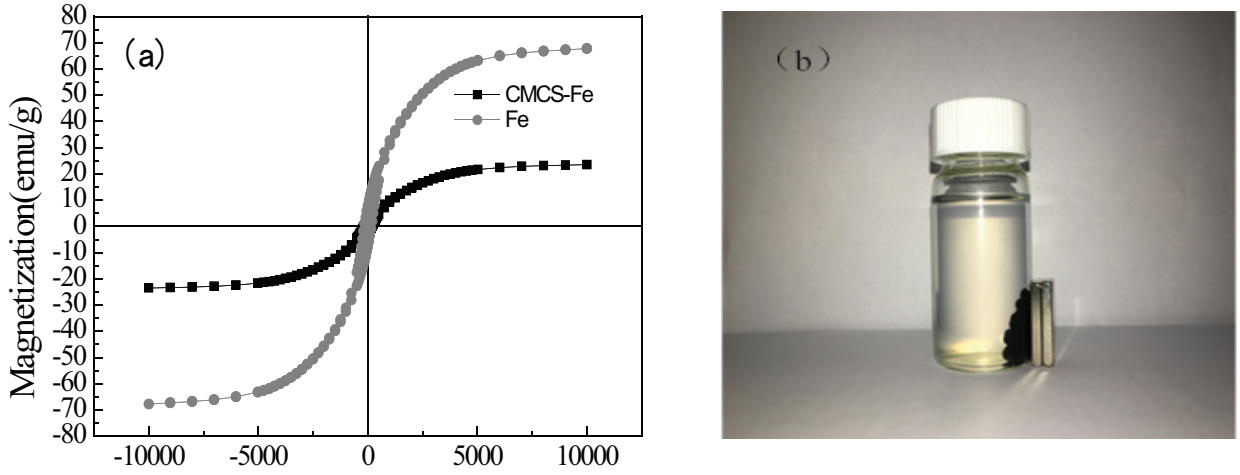

Fig. 3. VSM magnetization curves (a) and magnetic recovery of CMCS-nZVI beads (b).

were close to zero, which indicated that the CMCS-nZVI beads were super paramagnetic [35]. Fig. 3(a) shows that the saturation magnetization of the naked nZVI particles and the CMCS-nZVI beads are 67.8 and 23.5 emu/g, respectively. The saturation magnetization of the CMCS-nZVI beads was reduced to approximately one-third of the naked nZVI particles. Because *N*-carboxymethyl chitosan has no magnetism, the content of nZVI particles in the CMCS-nZVI beads was less than the naked nZVI particles with the same mass, which led to a decrease in saturation magnetization of the CMCS-nZVI beads [36,37]. Although the saturation magnetization of CMCS-nZVI beads decreased, it could also be separated magnetically and rapidly from the liquid phase, which would facilitate its use in practice.

3.4. Removal of Cr(VI) from water by CMCS-nZVI beads

3.4.1. Influence of CMCS-nZVI dosage on Cr(VI) removal

Fig. 4(a) shows the influence of CMCS-nZVI dosage on Cr(VI) removal with kinetic curves fitted in Fig. 4(b). For 50 mL of 10 mg/L Cr(VI) solution, the removal efficiency on Cr(VI) was enhanced with an increase in the amount of CMCS-nZVI beads. After a 1-h reaction, the removal rates of Cr(VI) were 37.83%, 48.54%, 62.22%, 74.55%, and 92.5%, respectively, when the CMCS-nZVI dosages were 0.12, 0.2, 0.4, and 0.6 g/L. The reactions tended to equilibrium after 8 h and the corresponding removal efficiencies of Cr(VI) reached 69.47%, 86.32%, 95.89%, 100%, and 100%, respectively. An increased dosage could reduce the reaction equilibrium time. For instance, when the CMCS-nZVI dosage increased to 0.6 g/L, the reaction reached equilibrium within 2 h. Fig. 4(a) compares the Cr(VI) removal by nZVI and CMCS-nZVI at a dosage of 0.6 g/L under other identical conditions. After 2 h, the Cr(VI) removal efficiency was 68% for bare nZVI, which suggests that the introduction of CMCS could increase the Cr(VI) removal efficiency.

Fig. 4(b) shows that the removal kinetic curves on Cr(VI) by CMCS-nZVI beads fitted the pseudo-first-order kinetic model well with $R^2 > 0.89$. The apparent reaction rate constants (K_{obs}) increased with an increase in CMCS-nZVI dosage. The K_{obs} increased from 0.0976 to 2.2302 h^{-1} when the CMCS-nZVI dosage increased from 0.12 to 0.6 g/L. This occurs because an increase in CMCS-nZVI bead dosage results in an increase in total surface area and the number of reactive sites on the CMCS-nZVI beads for Cr(VI), which enhances the opportunity for contact between Cr(VI) and CMCS-nZVI beads in solution and thus results in a relatively rapid reaction rate and a high removal efficiency [38]. Liu et al. [2] found that K_{obs} was linearly proportional to the CS-nZVI microsphere dosage. Wang et al. [20] showed that the Cr(VI) reduction rate increased with the addition of nanoiron particles that were coated with carboxymethyl cellulose.

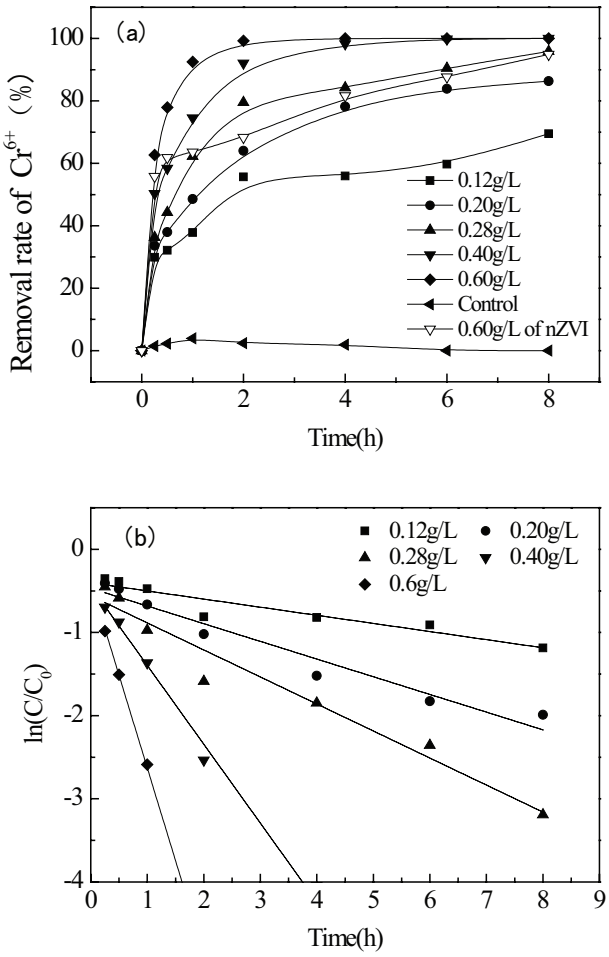

Fig. 4. Effects of dosage on Cr(VI) removal by CMCS-nZVI beads (a) and kinetic curves of Cr(VI) removal at different dosages (b). Initial [Cr^{6+}] = 10 mg/L, temperature = 25°C, and pH_0 = 6.6–6.9.

3.4.2. Influence of initial concentration on Cr(VI) removal

The effects of initial Cr(VI) concentration on Cr(VI) removal and kinetics at different initial concentrations are shown in Figs. 5(a) and (b), respectively. Fig. 5(a) shows that the removal efficiency of Cr(VI) by CMCS-nZVI beads decreased with an increase in initial Cr(VI) concentration.

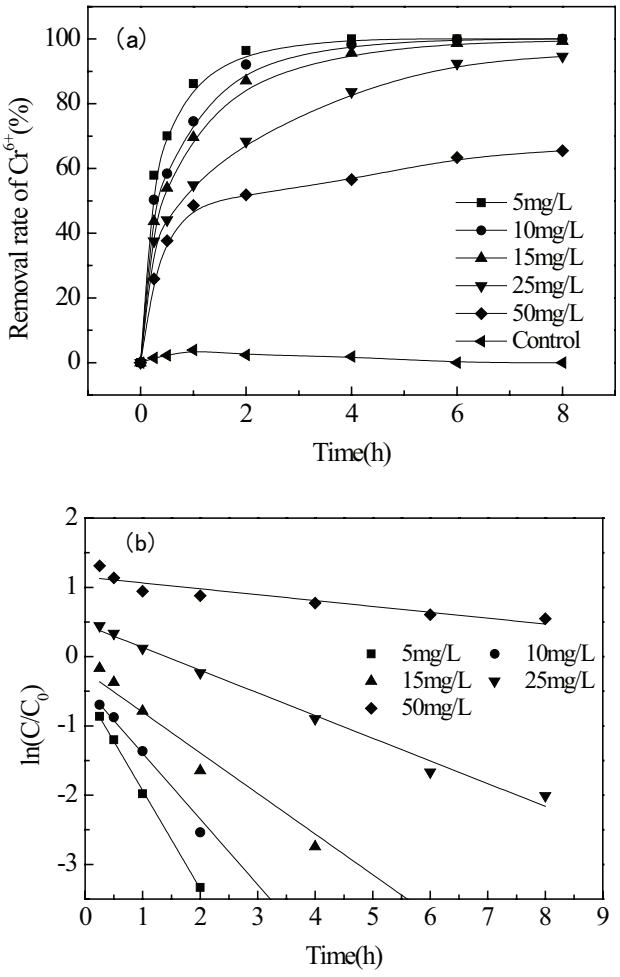

Fig. 5. Effects of initial concentration on Cr(VI) removal by CMCS-nZVI beads (a) and kinetic curves of Cr(VI) removal at different initial concentration (b). Temperature = 25°C, dose of CMCS-nZVI = 0.6 g/L, and pH_0 = 6.6–6.9.

After 2 h, the Cr(VI) removal efficiencies were 96.44%, 92.10%, 87.13%, 68.33%, and 51.83%, respectively, with initial concentrations of 5, 10, 15, 25, and 50 mg/L, respectively. Fig. 5(b) shows that the Cr(VI) removal kinetics was fitted to the pseudo-first-order kinetic model at different initial concentrations, and $R^2 > 0.85$. K_{obs} decreased with increasing initial Cr(VI) concentrations. When the initial concentration of Cr(VI) increased from 5 to 50 mg/L, the K_{obs} value decreased from 1.4172 to 0.0848 h^{-1}. Fu et al. [11] found that K_{obs} decreased with the concentration of Cr(VI) for sepiolite coated with nanoiron particles for Cr(VI) removal from groundwater. This occurred because the amount of CMCS-nZVI beads added into solution was constant and the number of total active sites was definite. When the Cr(IV) solution concentration increased, the active sites became occupied gradually and excess Cr(VI) could not be removed, which resulted in a reduction in removal efficiency [39,40]. The other reason is that Fe^0 could reduce Cr(VI) to Cr(III), and Fe^0 would be oxidized to Fe(II) or Fe(III) during the reaction. Fe(II)/Fe(III) and Cr(III) oxides/hydroxides coprecipitate from solution and deposit on the Fe^0 surface to form a passivation layer, which prevents the internal electron transfer of Fe^0 to outside and reduces the Cr(VI) removal rate [41].

3.4.3. Influence of initial pH on Cr(VI) removal

The effect of initial solution pH on Cr(VI) removal by CMCS-nZVI beads at different pH is shown in Fig. 6(a). The Cr(VI) removal efficiency decreased with increase in initial pH. When the initial solution pH values were 3.03, 7.02, and 10.97, the Cr(VI) removal efficiencies by the CMCS-nZVI beads were 100%, 99.39%, and 91.33%, respectively, after 6 h. Fig. 6(b) shows the kinetic curves of Cr(VI) removal at different pH. The Cr(VI) removal kinetics agreed with the pseudo-first-order kinetic model with all $R^2 > 0.95$. The K_{obs} of the reaction decreased with an increase in initial pH. When the pH was 3.03, 7.03, and 10.97, K_{obs} was 6.0513, 0.7675, and 0.3566 h^{-1}, respectively. An acidic environment could enhance the Cr(VI) removal by CMCS-nZVI because: (1) a lower pH favors Fe^0 corrosion and the formation of Fe(II)/Fe(III), and promotes Cr(VI) reduction; (2) acidic condition could hinder the formation of Fe(III)–Cr(VI) hydroxide coprecipitation, and weaken the by-effect of passivation; and (3) the surface charges of the beads becomes positive under acidic conditions, which is conducive to the electrostatic attraction to $HCrO_4^-$ anions [42,43].

3.4.4. Effect of reaction temperature on Cr(VI) removal

The influence of different reaction temperatures on Cr(VI) removal by CMCS-nZVI beads and the kinetic curves are shown in Fig. 7. Higher temperatures could shorten the reaction equilibrium time and increase the Cr(VI) removal rate, which indicates that Cr(VI) removal by CMCS-nZVI beads was endothermic. When the temperature was 25°C ± 1°C, 40°C ± 1°C, and 50°C ± 1°C, the Cr(VI) removal efficiencies were 92.10%, 97.05%, and 98.80% after 2 h, respectively. Fig. 7(a) shows that the kinetic curves for Cr(VI) removal by CMCS-nZVI beads at different reaction temperatures obeyed the pseudo-first-order kinetic model with all $R^2 > 0.98$. When the temperature increased from 25°C ± 1°C to 50°C ± 1°C, K_{obs} increased from 1.0675 to 1.8544 h^{-1}, which indicates that an increased temperature could promote the removal reaction.

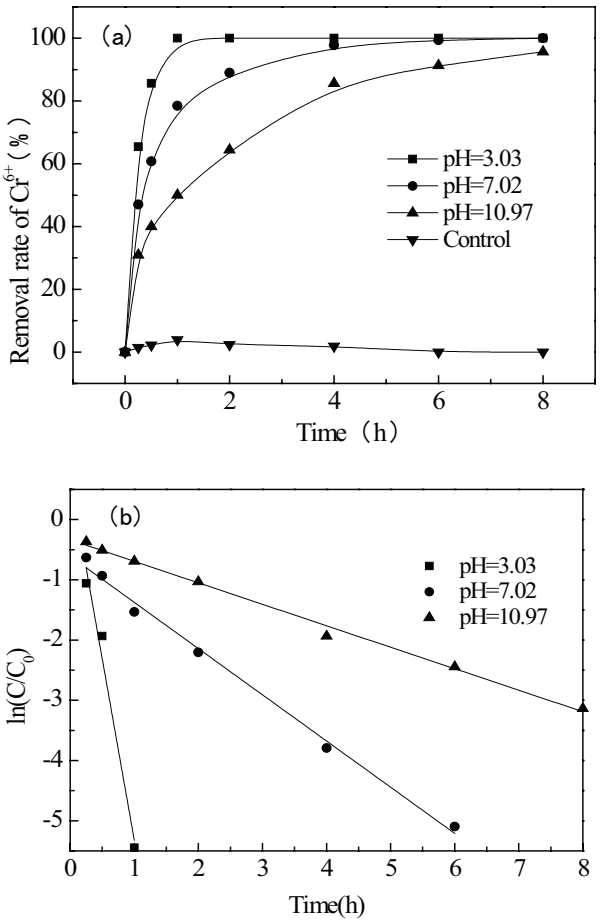

Fig. 6. Effects of pH on Cr(VI) removal by CMCS-nZVI beads (a) and kinetic curve of Cr(VI) removal at different pH (b). Initial [Cr^{6+}] = 10 mg/L, temperature = 25°C, and dose of CMCS-nZVI = 0.6 g/L.

To further evaluate the reaction mechanism, the experimental data in Fig. 7(b) were also plotted according to the linearized Arrhenius equation:

$$\ln K_{obs} = \ln A - \frac{E_a}{RT} \quad (1)$$

where A is the pre-exponential factor (h^{-1}), R is the universal gas constant (8.314 J/mol K), T is absolute temperature (K), and E_a is the activation energy (kJ/mol). From the linear plot of $\ln K_{obs}$ vs. $1/T$ in Fig. 7(b), the activation energy was calculated by the slope of the line. The Arrhenius equation agreed well with the experimental data and $R^2 = 0.9997$. The activation energy was approximately 22.99 ± 0.26 kJ/mol for Cr(VI) reduction by the CMCS-nZVI beads. The activation energy determined in this study was lower than that in the other reports. For instance, Talreja et al. [44] reported an activation energy of 87.41 kJ/mol by Fe-grown carbon nanofibers containing porous carbon microbeads to remove

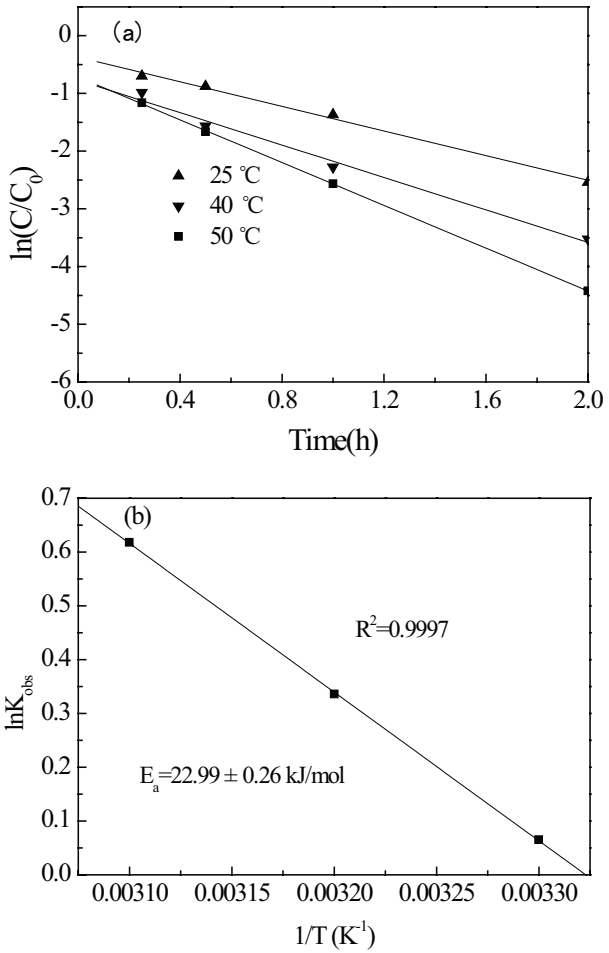

Fig. 7. Kinetic curve of Cr(VI) removal at different reaction temperature (a) and linearized Arrhenius plot of the K_{obs} as a function of $1/T$ (b). Initial [Cr^{6+}] = 10 mg/L, dose of CMCS-nZVI = 0.6 g/L, and pH_0 = 6.6–6.9.

hexavalent chromium at the temperatures ranging from 20°C to 40°C. It indicates that increased reaction temperature could improve the contaminant transfer rate, and increase the contact opportunity between Cr(VI) and CMCS-nZVI beads, which results in a higher removal efficiency [45].

3.5. FTIR analysis

To investigate the possible interaction between CMCS-nZVI beads and Cr(VI), FTIR spectra were obtained for CMCS-nZVI beads before and after reaction with Cr(VI) from 500 to 4,000 cm^{-1}, and the results are given in Fig. 8. For fresh CMCS-nZVI beads in Fig. 8(a), an obvious broad band from 3,500 to 3,200 cm^{-1} was attributed to peaks of O–H and N–H stretching vibrations in CMCS. The characteristic peak at 1,640 cm^{-1} corresponded to a C=O vibration that was conjugated with an N–H (amide I) deformation in CMCS [45–47]. Amide II, N–H, and C=N deformation bands ranging from 1,550 to 1,590 cm^{-1} were also observed. No free amine ($–NH_2$) existed at 1,605–1,580 cm^{-1} because one of the hydrogens on the amine group was substituted by a carboxymethyl group [23].

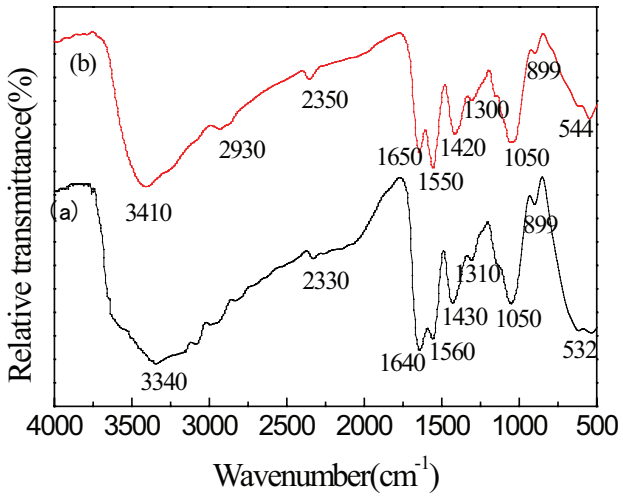

Fig. 8. FTIR images of CMCS-nZVI beads before (a) and after (b) reaction with Cr(VI).

Fig. 8(b) shows that compared with the fresh CMCS-nZVI beads, the FTIR spectra exhibited no significant changes after reaction with Cr(VI). However, the characteristic peaks of C=O and N–H shifted slightly to 1,650 and 1,550 cm^{-1}, respectively. The peak intensities of the O–H, C=O, and N–H vibration bands decreased visibly, which indicates that the carboxyl, amino, and hydroxyl groups in the CMCS may be chelated with iron ions or chromium ions. Other studies have indicated that the amide II, carboxyl, and hydroxyl groups in chitosan or CMCS showed a high adsorption capability for heavy metals [2,46,48]. Therefore, it is inferred that CMCS could enrich Cr(VI) on the surface or inside the CMCS-nZVI beads, and promote the contact and reaction between Cr(VI) and nZVI particles [2].

3.6. XRD analysis

Fig. 9(a) shows the XRD pattern of CMCS-nZVI beads before reaction with Cr(VI). The XRD profile of fresh CMCS-nZVI was amorphous because of the presence of CMCS. The characteristic diffraction peak appeared at a 2θ of 44.3°, which confirms the existence of zero-valent iron (Fe^0) in freshly prepared CMCS-nZVI [49]. Fig. 9(b) shows the XRD profile of CMCS-nZVI beads after reaction with Cr(VI). Compared with fresh CMCS-nZVI beads, the diffraction peak of Fe^0 at a 2θ of 44.3° weakened significantly, which suggests that the nZVI particles participated in the Cr(VI) removal reaction. One new diffraction peak at a 2θ of 35° was visible in the CMCS-nZVI beads after reaction, which indicates the presence of maghemite (Fe_2O_3), magnetite (Fe_3O_4), and Cr_2FeO_4 [50]. The other new diffraction peak at a 2θ of 62.2° was attributed to the Fe_3O_4 peak [11,51]. These results prove that after reaction with Cr(VI), the nZVI in the CMCS-nZVI beads was oxidized to Fe(II) and Fe (III), whereas the Cr(VI) was reduced mainly to Cr(III).

3.7. XPS analysis

Fig. 10(a) presents the XPS wide-scan of CMCS-nZVI beads before reaction with Cr(VI). The principal elements at

the surface of newly prepared CMCS-nZVI beads were Fe, O, and C and small amounts of N, Ca, and Cl were present. Elemental Fe was from freshly prepared nZVI, and elemental O, C, and N were attributed to the introduction of CMCS as a support. Elemental Ca and Cl were derived from the $CaCl_2$ cross-linking agent. Fig. 10(b) shows the XPS wide-scan of CMCS-nZVI beads after reaction with Cr(VI). One main difference between the freshly prepared CMCS-nZVI beads and the reacted CMCS-nZVI beads is that a new photoelectron peak emerged at 576.6 eV (Cr), which corresponds to the adsorption or reduction of chromium by CMCS-nZVI beads. A weak peak at 399.0 eV in Fig. 10(a) is attributed to elemental N in the $–NH_2$ groups. After Cr(VI) removal, the peak intensity of elemental N increased slightly in Fig. 10(b), which may occur because of the formation of metal–NH_2 complex (chelated with Fe and Cr). However, the peak intensity was low, which indicates that the amount of metal–NH_2 complex was limited [2,42].

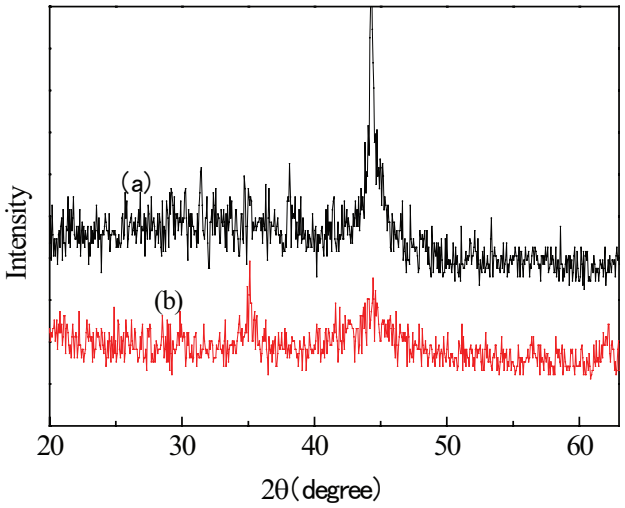

Fig. 9. XRD images of the CMCS-nZVI beads before (a) and after (b) reaction with Cr(VI).

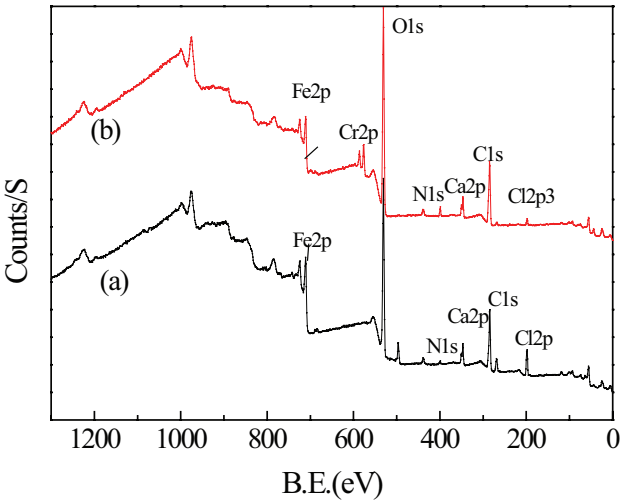

Fig. 10. XPS wide-scan survey of CMCS-nZVI before (a) and after (b) reaction with Cr(VI).

A detailed XPS survey on the region of the Fe 2p spectra for CMCS-nZVI beads before and after Cr(VI) removal is presented in Fig. 11. For fresh CMCS-nZVI, the peaks at 709.3 and 722.7 eV were assigned to Fe(II) oxide, and peaks

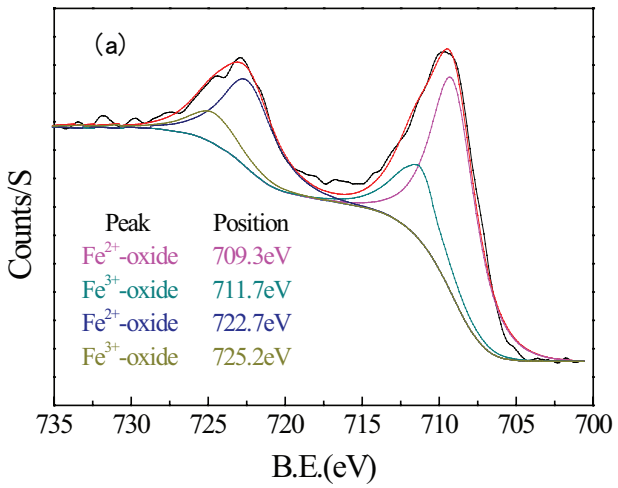

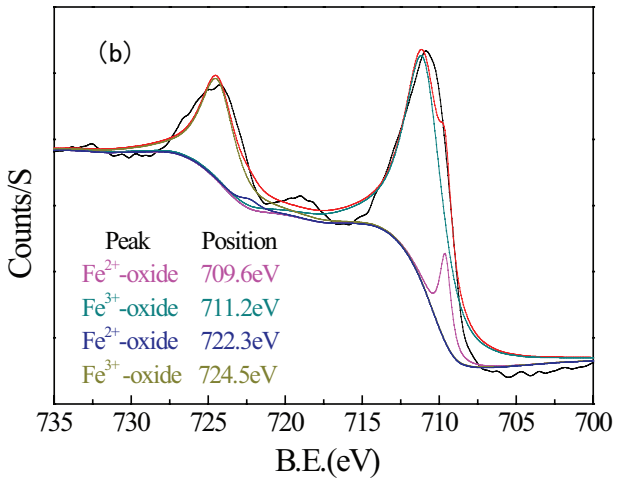

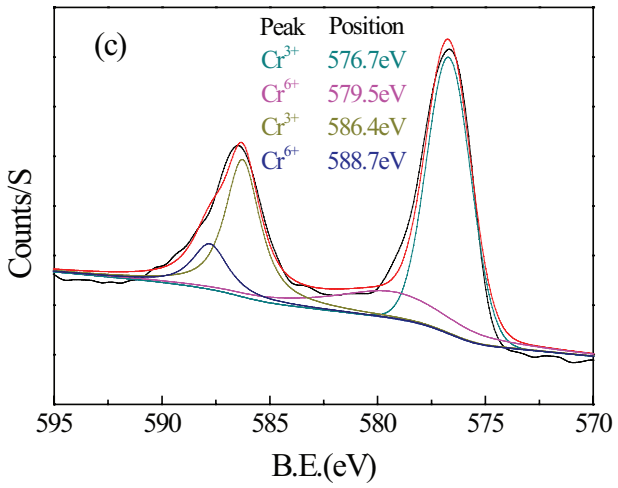

Fig. 11. Detailed XPS spectra of Fe 2p before reaction (a), Fe 2p after reaction (b), and Cr 2p after reaction (c).

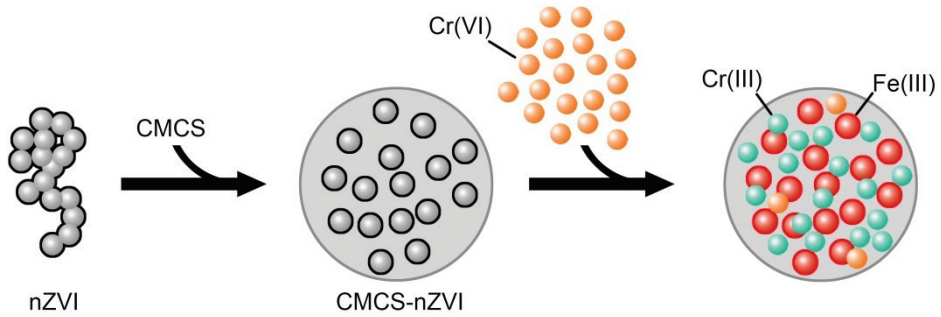

Scheme 1. The schematic representation of Cr(VI) removal mechanisms by CMCS-nZVI beads.

at 711.7 and 725.2 eV were attributed to binding energies of $2p_{3/2}$ and $2p_{1/2}$ of oxidized iron(III) [52,53]. Peaks of Fe^0 at 706 and 720 eV were not detected because of oxidation during transportation and detection, where X-rays could only penetrate less than 10 nm in the oxidized surface layer [2,54]. He and Zhao [18] also reported that Fe 2p peaks were not Fe^0, but were oxidized iron from XPS analysis. The intensities of Fe(II) oxide at 709.3 and 722.7 eV were greater than the Fe(III) oxides at 711.7 and 725.2 eV, which suggested that the surface of the fresh CMCS-nZVI was coated mainly by a shell of Fe(II) oxides. In contrast with the fresh CMCS-nZVI, after reaction with chromium, the intensity of the Fe(II) oxide peaks at 709.6 and 722.3 eV weakened visibly, whereas the Fe(II) oxide peaks at 711.2 and 724.5 eV strengthened significantly in Fig. 11(c). These changes suggest that most of the Fe^0 on or in the CMCS-nZVI beads was oxidized to Fe(III) after reaction, including Fe_2O_3, Fe_3O_4, and FeOOH [51].

Fig. 11(c) shows a detailed XPS survey on the region of the Cr 2p spectra for CMCS-nZVI beads after reaction with Cr(VI). Peaks at 576.6 and 586.4 eV were attributed to the binding energies of Cr $2p_{3/2}$ and Cr $2p_{1/2}$, which corresponded to Cr(III). The binding energies of Cr(VI) were characterized at 579.0 and 588.7 eV. Curve fitting indicated that, after reaction, 83.65% of the chromium species on the surface of the CMCS-nZVI beads were Cr(III), whereas 16.35% was Cr(VI). Therefore, most Cr(VI) was reduced to Cr(III) by CMCS-nZVI beads, and a small amount of Cr(VI) was retained, which was similar to the results reported by Genç-Fuhrman et al. [40] and Li et al. [41]. These results suggested that the reduction of Cr(VI) by nZVI was important in Cr(VI) removal, and the main product may be CrOOH, Cr_2O_3, Cr_2FeO_4, and $Cr(OH)_3$ [55]. A small part of the Cr(VI) residues may result from the chelation effect between reactive groups in the CMCS and Cr(VI) ions [41,42].

In brief, based on the FTIR, XRD, and XPS analyses, a possible removal mechanism of Cr(VI) by CMCS-nZVI beads is outlined as shown in Scheme 1. Because CMCS has rich reactive groups and nZVI has high reactivity, Cr(VI) could be enriched easily on the surface or transferred inside the CMCS-nZVI beads. Most Cr(VI) ions were reduced to Cr(III) by nZVI particles on the surface or inside of the CMCS-nZVI beads, whereas most of the nZVI was oxidized to Fe(III) after reaction. The main reaction products may be Fe_3O_4, Cr_2FeO_4, Fe_2O_3, FeOOH, CrOOH, Cr_2O_3, and $Cr(OH)_3$. A small portion of Cr(VI) was retained in the CMCS-nZVI beads by adsorption or chelation with the reactive groups in CMCS.

4. Conclusions

CMCS-supported nZVI nanoparticles were synthesized and used for Cr(VI) removal. CMCS introduction could improve the dispersive property and oxidation resistance of nZVI nanoparticles to a certain degree. An increased CMCS-nZVI bead dosage could enhance the Cr(VI) removal efficiency and shorten the reaction equilibrium time. For a 10 mg/L Cr(VI) solution, the Cr(VI) removal rates reached 100% with a dosage of 0.6 g/L in a 2 h reaction. A low solution pH favored Cr(VI) removal. A higher temperature shortens the reaction time and increases the Cr(VI) removal rate but the influence was insignificant. FTIR, XRD, and XPS analyses indicate that the possible Cr(VI) removal mechanism by CMCS-nZVI beads may be that the Cr(VI) in solution could be enriched on the surface or inside the CMCS-nZVI beads, and most Cr(VI) was reduced to Cr(III) by nZVI compared with adsorption/chelation of Cr(VI)/Cr(III) by CMCS.

Acknowledgment

This work was supported by grants from the Chinese National Natural Science Foundation (No. 51109019).

References

[1] H. Daraei, A. Mittal, J. Mittal, H. Kamali, Optimization of Cr(VI) removal onto biosorbent eggshell membrane: experimental and theoretical approaches, Desal. Wat. Treat., 52 (2014) 1307–1315.
[2] T. Liu, L. Zhao, D. Sun, Entrapment of nanoscale zero-valent iron in chitosan beads for hexavalent chromium removal from wastewater, J. Hazard. Mater., 184 (2010) 724–730.
[3] P. Baroni, R.S. Vieira, E. Meneghetti, S.M. Da, M.M. Beppu, Evaluation of batch adsorption of chromium ions on natural and cross linked chitosan membranes, J. Hazard. Mater., 152 (2008) 1155–1163.
[4] Q. Wang, H. Qian, Y. Yang, Z. Zhang, C. Naman, X. Xu, Reduction of hexavalent chromium by carboxymethyl cellulose-stabilized zero-valent iron nanoparticles, J. Contam. Hydrol., 114 (2010) 35–42.
[5] M. Miao, Y. Wang, Q. Kong, L. Shu, Adsorption kinetics and optimum conditions for Cr(VI) removal by activated carbon prepared from luffa sponge, Desal. Wat. Treat., 57 (2016) 7763–7772.
[6] E. Pérez, L. Ayele, G. Getachew, G. Fetter, P. Bosch, A. Mayoral, I. Diaz, Removal of chromium(VI) using nano-hydrotalcite/SiO_2 composite, J. Environ. Chem. Eng., 3 (2015) 1555–1561.
[7] S. Lameiras, C. Quintelas, T. Tavares, Biosorption of Cr(VI) using a bacterial biofilm supported on granular activated carbon and on zeolite, Bioresour. Technol., 99 (2008) 801–806.

[8] R. Singh, V. Misra, R.P. Singh, Removal of hexavalent chromium from contaminated ground water using zero-valent iron nanoparticles, Environ. Monit. Assess., 184 (2011) 3643–3651.
[9] Y. Qu, X. Zhang, J. Xu, W. Zhang, Y. Guo, Removal of hexavalent chromium from wastewater using magnetotactic bacteria, Sep. Purif. Technol., 136 (2014) 10–17.
[10] M.S. Mahmoud, S.A. Mohamed, Calcium alginate as an eco-friendly supporting material for Baker's yeast strain in chromium bioremediation, HBRC J., 2015 (2015) 1–10.
[11] F. Fu, W. Han, C. Huang, B. Tang, M. Hu, Removal of Cr(VI) from wastewater by supported nanoscale zero-valent iron on granular activated carbon, Desal. Wat. Treat., 51 (2013) 2680–2686.
[12] J. Liu, A. Liu, W. Zhang, The influence of polyelectrolyte modification on nanoscale zero-valent iron (nZVI): aggregation, sedimentation, and reactivity with Ni(II) in water, Chem. Eng. J., 303 (2016) 268–274.
[13] F. Fu, J. Ma, L. Xie, B. Tang, W. Han, S. Lin, Chromium removal using resin supported nanoscale zero-valent iron, J. Environ. Manage., 128 (2013) 822–827.
[14] Y. Xie, Z. Fang, X. Qiu, E.P. Tsang, B. Liang, Comparisons of the reactivity, reusability and stability of four different zero-valent iron-based nanoparticles, Chemosphere, 108 (2014) 433–436.
[15] K. Krzciuk, A. Gałuszka, Prospecting for hyperaccumulators of trace elements: a review, Crit. Rev. Biotechnol., 35 (2015) 522–532.
[16] A.N. Bezbaruah, S. Krajangpan, B.J. Chisholm, E. Khan, J.J. Bermudez, Entrapment of iron nanoparticles in calcium alginate beads for groundwater remediation applications, J. Hazard. Mater., 166 (2009) 1339–1343.
[17] L.M. Kustov, E.D. Finashina, E.V. Shuvalova, O.P. Tkachenko, O.A. Kirichenko, Pd-Fe nanoparticles stabilized by chitosan derivatives for perchloroethenede chlorination, Environ. Int., 37 (2011) 1044–1052.
[18] F. He, D. Zhao, Manipulating the size and dispersibility of zero valent iron nanoparticles by use of carboxymethyl cellulose stabilizers, Environ. Sci. Technol., 41 (2007) 6216–6221.
[19] H. Dong, I.M. Lo, Influence of humic acid on the colloidal stability of surface-modified nano zero-valent iron, Water Res., 47 (2013) 419–427.
[20] W. Wang, M. Zhou, Z. Jin, T. Li, Reactivity characteristics of poly(methyl methacrylate) coated nanoscale iron particles for trichloroethylene remediation, J. Hazard. Mater., 173 (2010) 724–730.
[21] H.K. How, Z.W.Y. Wan, Kaolinite-supported nanoscale zero-valent iron for removal of Pb^{2+} from aqueous solution: reactivity, characterization and mechanism, Water, 45 (2015) 3481–3488.
[22] W.S.W. Ngah, L.C. Teong, R.H. Toh, M.A.K.M. Hanafiah, Comparative study on adsorption and desorption of Cu(II) ions by three types of chitosan-zeolite composites, Chem. Eng. J., 223 (2013) 231–238.
[23] E. Guibal, C. Milot, O. Eterradossi, C. Gauffier, A. Domard, Study of molybdate ion sorption on chitosan gel beads by different spectrometric analyses, Int. J. Biol. Macromol., 24 (1999) 49–59.
[24] X. Weng, S. Lin, Y. Zhong, Z. Chen, Chitosan stabilized bimetallic Fe/Ni nanoparticles used to remove mixed contaminants-amoxicillin and Cd (II) from aqueous solutions, Chem. Eng. J., 229 (2013) 27–34.
[25] B.W. Zhu, T.T. Lim, J. Feng, Reductive dechlorination of 1,2,4-trichlorobenzene with palladized nanoscale Fe^0 particles supported on chitosan and silica, Chemosphere, 65 (2006) 1137–1145.
[26] Z. Liu, Y. Jiao, Z. Zhang, Calcium-carboxymethyl chitosan hydrogel beads for protein drug delivery system, J. Appl. Polym. Sci., 103 (2007) 3164–3168.
[27] J. Zhang, N. Chen, M. Li, C. Feng, Synthesis and environmental application of zirconium–chitosan/graphene oxide membrane, J. Taiwan. Inst. Chem. Eng., 77 (2017) 106–112.
[28] P. Wongpanit, N. Sanchavanakit, P. Pavasant, P. Supaphol, S. Tokura, R. Rujiravanit, Preparation and characterization of microwave-treated carboxymethyl chitin and carboxymethyl chitosan films for potential use in wound care application, Macromol. Biosci., 5 (2005) 1001–1012.
[29] F.G.L.M. Borsagli, A.A.P. Mansur, P. Chagas, L.C.A Oliveira, H.S. Mansur, *O*-carboxymethyl functionalization of chitosan: complexation and adsorption of Cd (II) and Cr (VI) as heavy metal pollutant ions, React. Funct. Polym., 97 (2015) 37–47.
[30] B. Mandal, S.K. Ray, Removal of safranine T and brilliant cresyl blue dyes from water by carboxy methyl cellulose incorporated acrylic hydrogels: isotherms, kinetics and thermodynamic study, J. Taiwan Inst. Chem. Eng., 60 (2016) 313–327.
[31] Y. Xie, Y. Yi, Y. Qin, L. Wang, G. Liu, Y. Wu, Z. Diao, T. Zhou, M. Xu, Perchlorate degradation in aqueous solution using chitosan-stabilized zero-valent iron nanoparticles, Sep. Purif. Technol., 171 (2016) 164–173.
[32] J.E. Martin, A.A. Herzing, W. Yan, X. Li, B.E. Koel, C.J. Kiely, W. Zhang, Determination of the oxide layer thickness in core-shell zero valent iron nanoparticles, Langmuir, 24 (2008) 4329–4334.
[33] N.A. Gujarathi, B.R. Rane, J.K. Patel, pH sensitive polyelectrolyte complex of O-carboxymethyl chitosan and poly (acrylic acid) cross-linked with calcium for sustained delivery of acid susceptible drugs, Int. J. Pharm., 436 (2012) 418–425.
[34] S. Li, G.W. Qin, Y. Zhang, W. Pei, L. Zuo, C. Esling, Anisotropic growth of iron oxyhydroxide nanorods and photo catalytic activity, Adv. Eng. Mater., 12 (2010) 1082–1085.
[35] H. Zhu, Y. Fu, R. Jiang, J. Yao, L. Xiao, G. Zeng, Novel magnetic chitosan/poly(vinyl alcohol) hydrogel beads: preparation, characterization and application for adsorption of dye from aqueous solution, Bioresour. Technol., 105 (2012) 24–30.
[36] D. Wu, J. Zhao, L. Zhang, Q. Wu, Y. Yang, Lanthanum adsorption using iron oxide loaded calcium alginate beads, Hydrometallurgy, 101 (2010) 76–83.
[37] A.S.A. Bakr, Y.M. Moustafa, E.A. Motawea, M.M. Yehia, M.M.H. Khalil, Removal of ferrous ions from their aqueous solutions onto $NiFe_2O_4$-alginate composite beads, J. Environ. Chem. Eng., 3 (2015) 1486–1496.
[38] B.A. Manning, J.R. Kiser, H. Kwon, S.R. Kanel, Spectroscopic investigation of Cr(III) and Cr(VI)-treated nanoscale zero-valent iron, Environ. Sci. Technol., 41 (2007) 586–592.
[39] T. Liu, X. Yang, Z. Wang, X. Yan, Enhanced chitosan beads-supported Fe^0-nanoparticles for removal of heavy metals from electroplating wastewater in permeable reactive barriers, Water Res., 47 (2013) 6691–6700.
[40] H. Genç-Fuhrman, P. Wu, Y. Zhou, A. Ledin, Removal of As, Cd, Cr, Cu, Ni, and Zn from polluted water using an iron based sorbent, Desalination, 226 (2008) 357–370.
[41] X. Li, J. Cao, W. Zhang, Stoichiometry of Cr(VI) immobilization using nanoscale zerovalent iron (nZVI): a study with high-resolution X-ray photo electron spectroscopy (HR-XPS), Ind. Eng. Chem. Res., 47 (2008) 2131–2139.
[42] B. Geng, Z. Jin, T. Li, X. Qi, Preparation of chitosan-stabilized Fe^0 nanoparticles for removal of hexavalent chromium in water, Sci. Total Environ., 407 (2009) 4994–5000.
[43] G.N. Jouvanovic, P. Plazl, P. Sakrittichal, K. Al-Khald, Dechlorination of *p*-chlorophenol in a microreactor with bimetallic Pb/Fe catalyst, Ind. Eng. Chem. Res., 44 (2005) 5099–5106.
[44] N. Talreja, D. Kumar, N. Verma, Removal of hexavalent chromium from water using Fe-grown carbon nanofibers containing porous carbon microbeads, J. Water Process Eng., 3 (2014) 34–45.
[45] T. Liu, Z. Wang, L. Zhao, X. Yang, Enhanced chitosan/Fe^0-nanoparticles beads for hexavalent chromium removal from wastewater, Chem. Eng. J., 189–190 (2012) 196–202.
[46] F. Mi, S. Wu, Y. Chen, Combination of carboxymethyl chitosan-coated magnetic nanoparticles and chitosan-citrate complex gel beads as a novel magnetic adsorbent, Carbohydr. Polym., 131 (2015) 255–263.
[47] G. Xia, X. Lang, M. Kong, X. Cheng, Y. Lin, C. Feng, X. Chen, Surface fluid-swellable chitosan fiber as the wound dressing material, Carbohydr. Polym., 136 (2016) 860–866.
[48] V.M. Boddu, K. Abburi, J.L. Talbott, E.D. Smith, Removal of hexavalent chromium from wastewater using a new composite chitosan biosorbent, Environ. Sci. Technol., 37 (2003) 4449–4456.
[49] F. Zhu, L. Li, S. Ma, Z. Shang, Effect factors, kinetics and thermodynamics of remediation in the chromium contaminated

soils by nanoscale zero valent Fe/Cu bimetallic particles, Chem. Eng. J., 302 (2016) 663–669.
[50] L. Shi, Y. Lin, X. Zhang, Z. Chen, Synthesis, characterization and kinetics of bentonite supported nZVI for the removal of Cr(VI) from aqueous solution, Chem. Eng. J., 171 (2011) 612–617.
[51] Z. Diao, X. Xu, D. Jiang, L. Kong, Y. Sun, Y. Hu, Q. Hao, H. Chen, Bentonite-supported nanoscale zero-valent iron/persulfate system for the simultaneous removal of Cr(VI) and phenol from aqueous solutions, Chem. Eng. J., 302 (2016) 213–222.
[52] C.M. Cirtiu, T. Raychoudhury, S. Ghoshal, A. Moores, Systematic comparison of the size, surface characteristics and colloidal stability of zero valent iron nanoparticles pre- and post-grafted with common polymers, Colloids Surf., A, 390 (2011) 95–104.
[53] B. Schnyder, D. Alliata, R. Kötz, H. Siegenthaler, Electrochemical intercalation of perchlorate ions in HOPG: an SFM/LFM and XPS study, Appl. Surf. Sci., 173 (2001) 221–232.
[54] H. Kim, H.J. Hong, J. Juri, S.H. Kim, J.W. Yang, Degradation of trichloroethylene (TCE) by nanoscale zero-valent iron (nZVI) immobilized in alginate bead, J. Hazard. Mater., 176 (2010) 1038–1043.
[55] L. Wu, L. Liao, G. Lv, F. Qin, Y. He, X. Wang, Micro-electrolysis of Cr(VI) in the nano scale zero-valent iron loaded activated carbon, J. Hazard. Mater., 254–255 (2013) 277–283.